

Synthesis and physical and magnetic properties of CuAlCr₄S₈: A Cr-based breathing pyrochloreS. Sharma¹, M. Pocrnic¹, B. N. Richtig², C. R. Wiebe^{2,3}, J. Beare¹, J. Gautreau¹, J. P. Clancy^{1,4}, J. P. C. Ruff⁵, M. Pula¹, Q. Chen^{1,4}, S. Yoon^{6,7}, Y. Cai^{6,8} and G. M. Luke^{1,6,*}¹*Department of Physics and Astronomy, McMaster University, Hamilton, Ontario, Canada L8S 4M1*²*Department of Chemistry, University of Manitoba, Winnipeg, Canada R3T 2N2*³*Department of Chemistry, University of Winnipeg, Winnipeg, Canada R3B 2E9*⁴*Brockhouse Institute for Materials Research, McMaster University, Hamilton, Ontario, Canada L8S 4M1*⁵*Cornell High Energy Synchrotron Source, Cornell University, Ithaca, New York 14853, USA*⁶*TRIUMF, Vancouver, British Columbia, Canada V6T 2A3*⁷*Department of Physics, Sungkyunkwan University, Suwon 16419, Korea*⁸*Quantum Matter Institute, The University of British Columbia, Vancouver, British Columbia, Canada V6T 1Z4*

(Received 12 January 2022; revised 24 March 2022; accepted 27 June 2022; published 12 July 2022)

We present the synthesis and physical properties of a breathing pyrochlore magnet CuAlCr₄S₈ via synchrotron x-ray diffraction, magnetization under ambient and applied hydrostatic pressure, heat capacity, and muon spin relaxation/rotation measurements. CuAlCr₄S₈ exhibits positive thermal expansion with a concave upward temperature dependence. We observed a sharp antiferromagnetic ordering transition of a purely magnetic nature at 20 K, which shifts by as much as 3.2 K on application of 600 MPa pressure. The breathing factor ($B_f = J'/J$) in breathing pyrochlores can be an important parameter to tune the magnetic ground states of the pyrochlore lattice. The breathing factor can be modulated through the breathing ratio, the ratio of the sizes of the two tetrahedra, by using different elements at the A and A' sites in the breathing pyrochlore structure. We find that CuAlCr₄S₈ has a breathing ratio of 1.0663(8), which is comparable to other sulfur breathing pyrochlores.

DOI: [10.1103/PhysRevB.106.024407](https://doi.org/10.1103/PhysRevB.106.024407)**I. INTRODUCTION**

Geometrically frustrated magnetic systems have been studied extensively over the last three decades [1]. The frustration between magnetic moments at corner sharing triangular or tetrahedral units can give rise to exotic ground states such as spin liquid [2], ordered and disordered spin ice [3,4], spin glass freezing [5], and order by disorder [6], to name a few. The chromium spinels with formulas ACr₂X₄ are a family of such compounds where magnetic chromium atoms sit on corner sharing tetrahedra allowing various novel states, including a zero-energy excitation mode in the spin liquid phase, heavy fermionic behavior, zero field, and field-induced transitions [7]. The presence of two different types of nonmagnetic elements at the A site leads to the formation of compounds with formulas AA'B₄X₈ and may lead to A-site ordering, which can allow the formation of larger and smaller tetrahedra. This structure with an alternating array of small and large tetrahedra is called the breathing pyrochlore structure. A breathing pyrochlore forms by displacement of the octahedral B-site cation and ordering of X anions [8]. This reduces the symmetry of the lattice, converting the centrosymmetric $F\bar{d}3m$ (227) structure into noncentrosymmetric $F\bar{4}3m$ (216), which belongs to the same group. This lowered symmetry allows additional reflections such as (200), (420), (600), etc., in the diffraction pattern, which are forbidden otherwise.

Numerous mixed A-site pyrochlores have been synthesized in the past with some examples of the A-site ordering [9–18]. Since the type of interaction between nearest-neighbor chromium atoms is distance sensitive, changing from strongly antiferromagnetic in an oxide spinel to ferromagnetic in a selenium spinel [19], the magnetic Cr³⁺ atoms at the edges of larger and smaller tetrahedra have different interactions. Along with the antiferromagnetic direct interaction between nearest-neighbor spins, ferromagnetic superexchange interactions between next-nearest-neighbor spins also play an important role in deciding the sign and magnitude of the overall dominant interactions [20,21].

The Heisenberg spin Hamiltonian for a breathing pyrochlore can be written as

$$H = J \sum_{ij} S_i S_j,$$

where $J \in \{J, J', J_{\text{nnn}}\}$. J and J' are exchange coupling constants for small and large tetrahedra, respectively and J_{nnn} is the interaction parameter between next-nearest-neighboring spins. Therefore, the breathing factor $B_f = J/J'$ can be an important parameter to tune different ground states.

Cr-based spinels with nonmagnetic A-site atoms tend to show strong magnetoelastic effects. For example, the structural transitions in ZnCr₂S₄ [22] and ZnCr₂Se₄ [23] as well as the negative thermal expansion of LiGaCr₄S₈ [24] can be explained via of magnetoelastic coupling. This unique combination of magnetic frustration along with bond alternation and magnetoelastic effects in the breathing pyrochlores allows

*luke@mcmaster.ca

them to host exotic phases including a classical spin nematic transition in $\text{LiGa}_{0.95}\text{In}_{0.05}\text{Cr}_4\text{O}_8$ [25], cluster frustration and negative thermal expansion in $\text{LiGaCr}_4\text{S}_8$ [20,24], and a spin gap transition and magnetostructural transition in $\text{LiFeCr}_4\text{S}_8$ [26]. These are a few examples of the diverse set of properties [27–32] exhibited by the breathing pyrochlores.

We study the $\text{CuAlCr}_4\text{S}_8$ system that was first synthesized by Pinch *et al.* [33] in 1970, reporting *A*-site ordering in the normal pyrochlore structure. We have successfully synthesized $\text{CuAlCr}_4\text{S}_8$ in the breathing pyrochlore structure. In this structure, nonmagnetic Cu^{1+} and Al^{3+} ions occupy the tetrahedral sites, whereas the Cr^{3+} ions populate the octahedral sites, forming an array of corner sharing tetrahedra in the pyrochlore lattice. The Cr^{3+} ion in Cr breathing pyrochlores adopts a $\text{spin-}\frac{3}{2}$ state due to the half-filled t_{2g} orbital, which leads to the formation of an ideal $\text{spin-}\frac{3}{2}$ system with strong geometric frustration.

II. EXPERIMENTAL DETAILS

The polycrystalline sample of $\text{CuAlCr}_4\text{S}_8$ was synthesized by the conventional solid-state reaction method. We used high-purity copper, aluminum, chromium, and sulfur powders from Alfa Aesar in stoichiometric ratios and ground them into a pellet, which was sealed in a quartz tube under 10 mTorr of argon pressure. We heated the sealed tube at 1000 °C in a box furnace for 48 h. This process was repeated at 1100 °C after being ground and pressed for a second time.

We performed preliminary room-temperature powder x-ray diffraction measurements using a Panalytical X'pert diffraction instrument, which uses a copper source with a wavelength of 1.540 56 Å. A Rietveld refinement of the XRD pattern was performed using the FULLPROF suite. The sample contained 4.3% weakly ferromagnetic Cr_3S_4 [34], which does not interfere with our measurements except for magnetic susceptibility measurements in low fields. Magnetization measurements were performed using a Quantum Design superconducting quantum interference device (SQUID) with a Reciprocating Sample Option (RSO) insert. We utilized a GC10/3 helium gas pressure cell from the Institute of High Pressure Physics, Polish Academy of Sciences, inserted into the magnetic property measurement system (MPMS) to allow for magnetization measurements under pressure up to 600 MPa, above 2 K. We performed specific heat measurements with a Quantum Design 9-T physical property measurement system (PPMS). Synchrotron x-ray diffraction measurements were carried out on a powder sample of $\text{CuAlCr}_4\text{S}_8$ using the QM2 beamline at the Cornell High Energy Synchrotron Source (CHESS). Measurements were performed using x rays with an incident energy of 29.20 keV ($\lambda = 0.424\,60$ Å), and a Pilatus 6M area detector. The sample was loaded into a borosilicate glass capillary (0.5 mm diameter), and cooled with a liquid helium cryostream. Measurements were carried out from a base temperature ($T = 12$ K) up to 300 K. Zero- and longitudinal-field muon spin relaxation/rotation (μSR) measurements were performed at the TRIUMF's LAMPF spectrometer on the M20 beamline. The μSR data were fitted with the help of the MUSRFIT software [35].

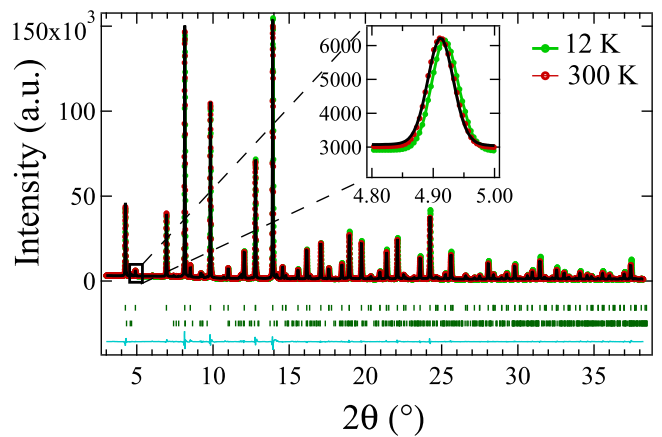


FIG. 1. The figure shows the fit of the synchrotron powder x-ray diffraction data taken at 300 and 12 K. There is a small shift in the intensities and peak positions between the two temperatures, but no different peaks occur at the different temperatures. The inset shows the zoomed view of the [200] peak, characteristic of the breathing pyrochlore structure, presenting evidence for a small shift in 2θ between the two scans.

III. RESULTS AND DISCUSSION

A. Synchrotron x-ray diffraction

The powder x-ray diffraction data taken 12 and 300 K on the polycrystalline samples of $\text{CuAlCr}_4\text{S}_8$ are shown in Fig. 1. Rietveld refinement of the XRD data reveals good agreement with the breathing pyrochlore structure with space group $F\bar{4}3m$. This crystal structure carries magnetic Cr^{3+} atoms at the corners of two unequal sized tetrahedra, unlike the normal pyrochlore (space group $F\bar{d}3m$) structure. The two Cr-Cr distances are 3.4020(14) and 3.6275(14) Å for this system. The ratio of the sizes of the two tetrahedra is called the breathing ratio B_r , which is 1.0663(8) for $\text{CuAlCr}_4\text{S}_8$. This value is comparable to other sulfide breathing pyrochlores such as $\text{CuInCr}_4\text{S}_8$ (1.06) [36], $\text{LiGaCr}_4\text{S}_8$ (1.077) [24], and so on, however, it is much less than the rare-earth compound $\text{Ba}_3\text{Yb}_2\text{Zn}_5\text{O}_{11}$ (1.90) [37], where the tetrahedra are decoupled.

$\text{CuAlCr}_4\text{S}_8$ retains the room-temperature crystal structure upon cooling to 12 K. However, the Bragg peaks exhibit broadening at the lowest temperature as shown in Fig. 2 (bottom). The crystallographic parameters at 300 and 12 K are listed in Tables I and II, respectively. The lattice parameters as a function of temperature, obtained from the Rietveld refinement, are shown in Fig. 2 (top). It shows a positive thermal expansion coefficient with a concave upward temperature dependence, unlike $\text{LiInCr}_4\text{S}_8$ and $\text{LiGaCr}_4\text{S}_8$, which show a concave downward temperature dependence with positive thermal expansion and negative thermal expansion, respectively [24,36,38]. The negative thermal expansion can arise due to competition between ferromagnetic and antiferromagnetic interactions through strong coupling with bond lengths, and its absence in $\text{CuAlCr}_4\text{S}_8$ means a weaker magnetoelastic coupling. The different types of temperature dependence of thermal expansion coefficients among the breathing pyrochlores likely originate from the varying strengths of magnetoelastic coupling.

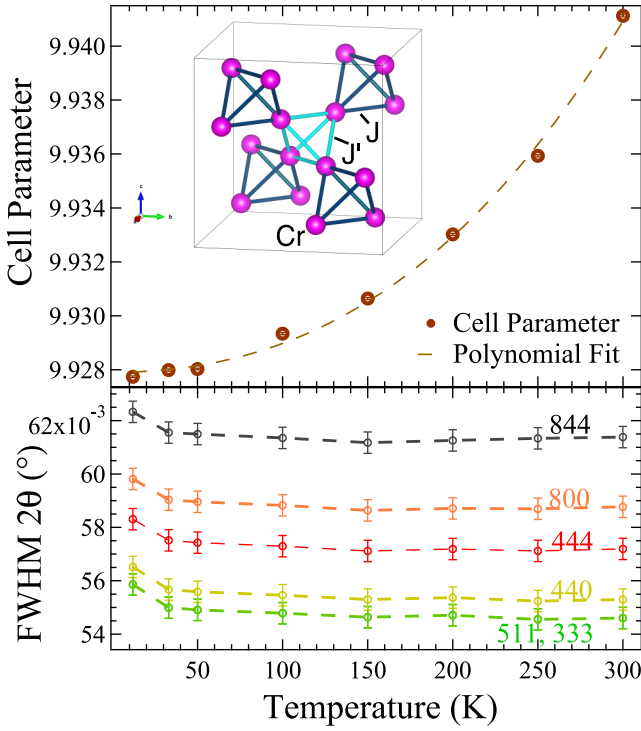


FIG. 2. Top: The temperature dependence of the unit cell parameter obtained from the Rietveld refinement is shown. Inset: The breathing pyrochlore lattice formed by Cr atoms where the smaller and larger tetrahedra are distinguished through different colored bonds. Bottom: The full width at half maximum (FWHM) for the labeled Bragg peaks as a function of temperature is shown. The width of the Bragg peaks shows an increase in cooling from 33 to 12 K, which indicates broadening associated with the magnetic ordering.

B. Magnetization

The dc magnetic susceptibility data in Fig. 3 show an upturn at 80 K in the low field (0.01 T), which could be due to the Cr_3S_4 impurity phase discussed earlier. $\text{CuAlCr}_4\text{S}_8$ undergoes a sharp dip in the magnetic susceptibility at 20 K. Moreover, no evidence of structural distortions associated with the magnetic susceptibility anomaly was observed in our synchrotron XRD measurements. The negative Curie-Weiss temperature obtained from the Curie-Weiss fit of the magnetic susceptibility establishes the dominant antiferromagnetic interaction in

TABLE I. The crystallographic parameters of $\text{CuAlCr}_4\text{S}_8$ determined by Rietveld refinement of the synchrotron XRD data at 300 K. The space group is $F\bar{4}3m$. The lattice parameters are $a = b = c = 9.94112(3)$ Å and B is the thermal factor.

		$x = y = z$	B (Å ²)	Occupancy
Cu1	4d	0.00000	0.380(75)	0.006(0)
Cu2	4a	0.75000	0.747(30)	1.007(1)
Al1	4d	0.00000	0.380(75)	0.994(1)
Al2	4a	0.75000	0.747(30)	0.006(0)
Cr	16e	0.37901(7)	0.416(11)	1
S1	16e	0.13210(6)	0.241(28)	1
S2	16e	0.61686(9)	0.421(27)	1

TABLE II. The crystallographic parameters of $\text{CuAlCr}_4\text{S}_8$ determined by Rietveld refinement of the synchrotron XRD data at 12 K. The space group is $F\bar{4}3m$. The lattice parameters are $a = b = c = 9.92774(3)$ Å and B is the thermal factor.

		$x = y = z$	B (Å ²)	Occupancy
Cu1	4d	0.00000	0.061(65)	0.006(0)
Cu2	4a	0.75000	0.118(24)	1.007(1)
Al1	4d	0.00000	0.061(65)	0.994(1)
Al2	4a	0.75000	0.118(24)	0.006(0)
Cr	16e	0.37906(6)	0.115(10)	1
S1	16e	0.13210(5)	-0.036(25)	1
S2	16e	0.61687(8)	0.121(24)	1

this system. The antiferromagnetic ordering temperature T_N of $\text{CuAlCr}_4\text{S}_8$ is comparable to the other antiferromagnetic samples of this sulfide family such as $\text{CuInCr}_4\text{S}_8$ (28 K) and $\text{LiGaCr}_4\text{S}_8$ (10.3 K) [36]. The magnetic transition shifts to a higher temperature upon application of hydrostatic pressure as shown in Fig. 4. The shift in transition displays an almost linear dependence on pressure, with 600 MPa inducing a 3.2-K increase in the Néel temperature as shown in Fig. 4 (inset). This may be due to the changing volume of the crystalline lattice induced by hydrostatic pressure, which generates stronger

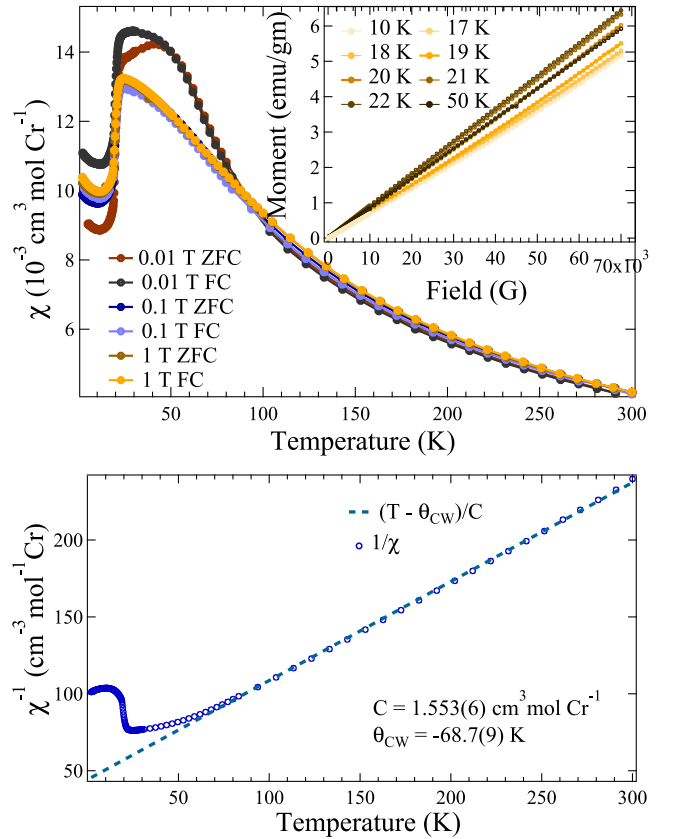


FIG. 3. Top: The dc magnetic susceptibility measurements on $\text{CuAlCr}_4\text{S}_8$. A sharp dip at 20 K in the magnetic susceptibility χ represents the antiferromagnetic transition. Bottom: The inverse susceptibility measured in the 0.1-T field and its Curie-Weiss fit in the temperature range 70–100 K. Inset: The $M-H$ at various temperatures around the magnetic transition are plotted.

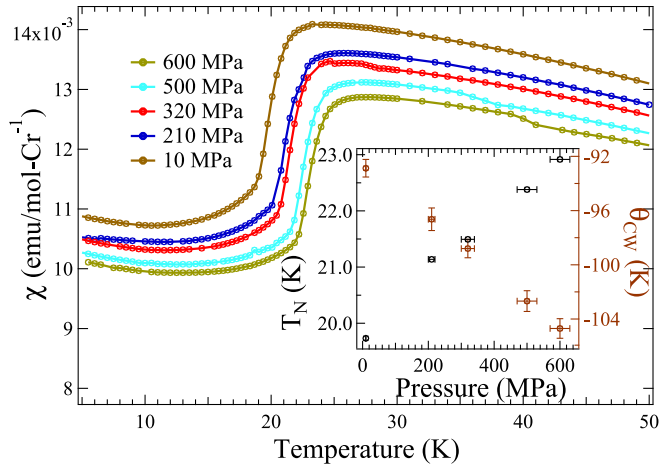


FIG. 4. The graph shows the magnetic susceptibility plots measured with 0.1 T applied field under different pressures. The inset shows the plot of midpoints of the magnetic transition and Curie-Weiss temperature against applied pressure

interactions among the magnetic spins, allowing for a higher magnetic ordering transition temperature. Magnetic susceptibility data were fit with the Curie-Weiss equation in the high-temperature range (70–300 K) as shown in Fig. 3(b),

$$\chi(T) = \frac{C}{T - \theta_{CW}}, \quad (1)$$

where $C = N_A g^2 \mu_B^2 S(S+1)/3k_B$. The value of the Curie-Weiss constant [$C = 1.553(6)$ emu K/mol] obtained from the fits of the ambient pressure data corresponds to an effective magnetic moment (μ_{eff}) of $3.525(7)\mu_B$, which is lower than the other sulfide breathing pyrochlores. This value of μ_{eff} yields a $g = 1.83$ for $S = 3/2$. The Curie-Weiss temperature (θ_{CW}) for $\text{CuAlCr}_4\text{S}_8$ is $-68.7(9)$ K. The smaller value of the Néel temperature in comparison to the Weiss temperature signifies the suppressed antiferromagnetic (AFM) long-range interactions due to frustration. The frustration factor ($T_f = \theta_{CW}/T_N$) for $\text{CuAlCr}_4\text{S}_8$ is $3.43(7)$. The Curie-Weiss fit of the 600-MPa data exhibits the same Curie-Weiss constant (within the error limit) as the ambient pressure data, implying the unchanged effective moment. However, the Curie-Weiss temperature has negative linear dependence on pressure as shown in Fig. 4 (inset).

C. Heat capacity

Heat capacity measurements performed on a polycrystalline sample of $\text{CuAlCr}_4\text{S}_8$ are shown in Fig. 5. There is a sharp peak in heat capacity data at 20 K, which is independent of the applied field (up to 7 T). The bottom panel of the figure depicts the total entropy as a function of temperature. Due to the absence of the nonmagnetic analog of this sample, we could not subtract the lattice contribution from the entropy. The system is not able to recover the full entropy of a spin- $3/2$ magnetic system until 40 K, despite not correcting for the lattice contribution. The temperature derivative of magnetic susceptibility manifests the same behavior as specific heat near the magnetic transition (Fig. 5, top), which in principle looks antiferromagnetic; however, a detailed neutron diffrac-

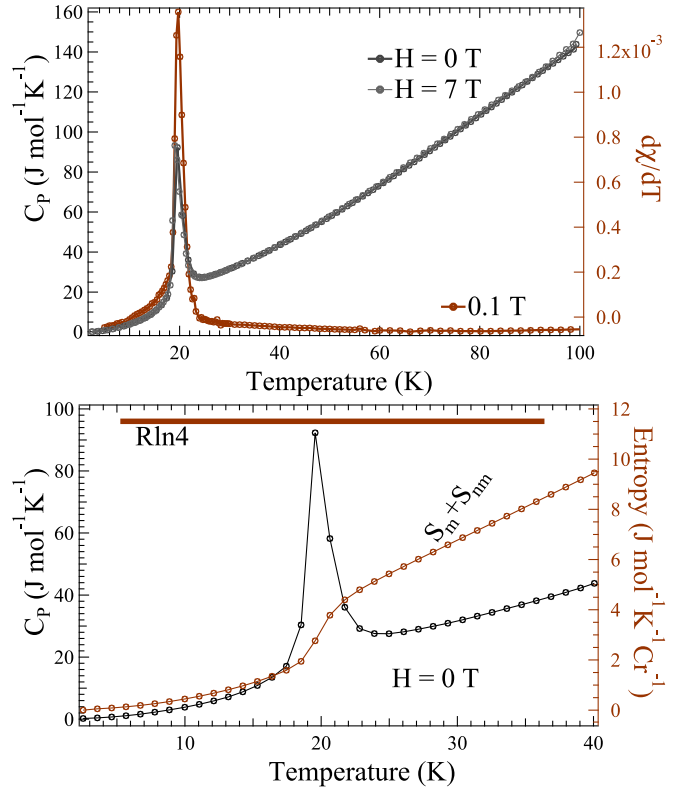


FIG. 5. Top: The figure shows that the sample heat capacity and the slope of the magnetic susceptibility peak at the same temperature. Bottom: The expanded view of zero-field heat capacity to elucidate the near T_N ranges. The total entropy (magnetic+nonmagnetic) and the maximum entropy of a spin- $3/2$ system are shown here for comparison

tion experiment is desired to definitely determine the nature of the magnetic ground state.

D. Zero-field (ZF)/longitudinal-field (LF) muon spin relaxation/rotation (μSR)

Figure 6(a) shows zero-field μSR spectra taken at temperatures between 2 and 100 K. The relaxation rate starts increasing as we cool down from 100 K and the majority of the signal relaxes out on going through the magnetic transition. We do not see any spontaneous oscillations in the signal in the ordered state, in contrast to what was seen with $\text{LiGaCr}_4\text{O}_8$ [39] and ZnCr_2O_4 [40]. The fast relaxing part of the signal is fit with an exponentially relaxing function, whereas the 1/3 tail is fit with a stretched exponential function as shown in Eq. (2),

$$A = \frac{A_0}{3} e^{-(\lambda_1 t)^\beta} + \frac{2A_0}{3} e^{-\lambda_2 t}, \quad (2)$$

where A is the total asymmetry and A_0 is the initial asymmetry. λ_1 and λ_2 are fast and slow relaxation rates, respectively. β is the exponent of the stretched exponential factor fitting to the 1/3 tail of the signal. In a polycrystalline sample, the local field points in random directions, where the 1/3 component of the signal describes the spins parallel to the initial muon spin while the remaining 2/3 part describes the spins perpendicular to the initial muon spin direction. The monotonically

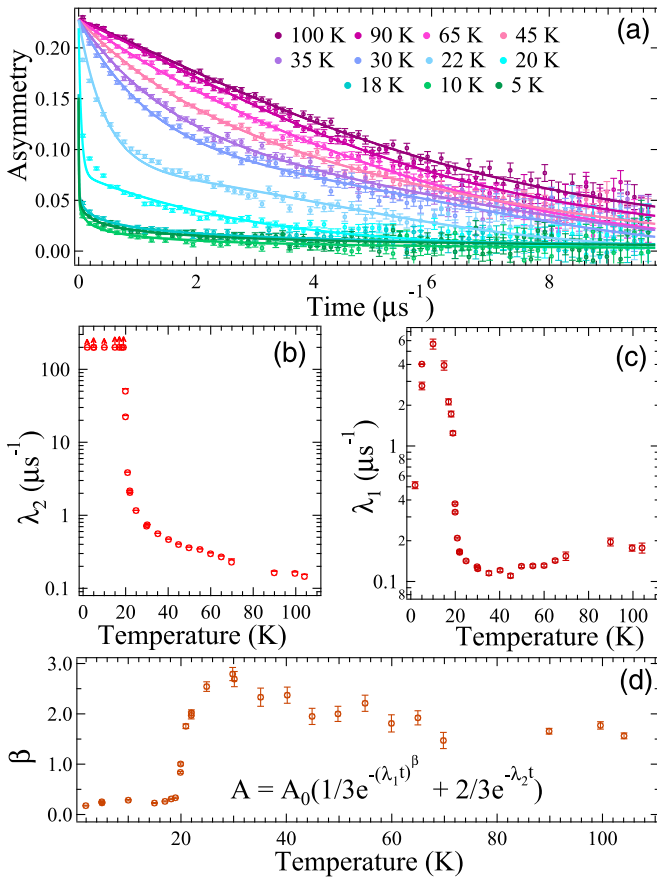


FIG. 6. The zero-field (ZF) μ SR data taken on a polycrystalline sample of $\text{CuAlCr}_4\text{S}_8$. (a) The asymmetry spectra taken at various temperatures above and below the T_N . The relaxation rates (b) λ_1 and (c) λ_2 , and (d) stretched exponential factor β as obtained from the fits of the asymmetry are plotted against temperature. All three parameters show an abrupt change of relaxation rates as we cool down the sample below its ordering temperature. The relaxation rate λ_2 is too fast below 20 K and constrained to be less than $200 \mu\text{s}^{-1}$ and therefore poorly determined.

increasing relaxation rates upon cooling signify the slowing down of spin fluctuations. Upon cooling below 20 K, the asymmetry signal starts to decay rapidly. The relaxation rates rise sharply, indicating quasistatic magnetic ordering at 20 K. The fact that we have 1/3 and 2/3 components means that the entire sample undergoes spin freezing. The internal field below $T_N = 20$ K is very large and as such we are unable to resolve the time dependence of the muon polarization, either to detect oscillations as would be expected in an ordered state, or a nonoscillating but rapidly relaxing signal as would be expected in a glassy state.

We also performed longitudinal-field (LF) μ SR measurements. In the longitudinal-field μ SR experiment, a field is applied parallel to the initial muon spin and this field cants the magnetic moments along the magnetic field, making the perpendicular field smaller, and the effective parallel field larger, thereby shifting the 1/3 tail upward for the polycrystalline samples. This process brings some of the fast relaxing asymmetry signal in the μ SR time window. Figure 7 shows the asymmetry spectra of the sample under different applied fields. The longitudinal field of 4 kG shifts the μ SR spectra

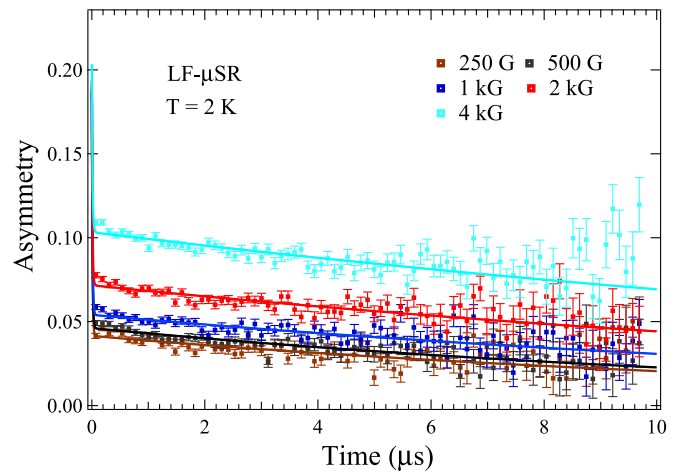


FIG. 7. Longitudinal-field (LF) μ SR data taken on a polycrystalline sample of $\text{CuAlCr}_4\text{S}_8$ under different fields show an upward shift of the 1/3 tail.

up, however, it is not enough to bring the entire fast relaxing component of the signal in the μ SR time window. This implies that the characteristic internal fields are quasistatic and are of the order of few thousand gauss.

IV. DISCUSSION

The sharp nature of the transition in both magnetic susceptibility and specific heat suggests the possibility of a first-order transition. However, the absence of any temperature hysteresis in magnetic susceptibility and the observation of no significant change of cell volume detected across the transition makes a definitive statement impossible. It is possible that the magnetoelastic coupling is too weak to give observable effects in the cell volume.

As evident from Fig. 1, we do not observe any peak splitting or any new peaks arising below the magnetic transition; this implies that the structure retains cubic symmetry. We do, however, see a subtle peak broadening below the magnetic transition, as shown in Fig. 2, which exhibits no particular HKL dependence, suggesting no change of symmetry. This broadening may correspond to very small distortions or structural fluctuations which cannot be resolved with the current resolution of the data. This could be investigated in more detail with higher-resolution synchrotron measurements, with measurements on single-crystal samples (if available in the future), or through more detailed temperature-dependent data.

V. CONCLUSION

We successfully synthesized a breathing pyrochlore material $\text{CuAlCr}_4\text{S}_8$, and investigated structural and magnetic properties. The specific heat data exhibit a sharp peak at 20 K, which is supported by an abrupt dip in the magnetic susceptibility. We observe a linear increase in magnetic transition at a rate of 0.53 K/kbar of applied helium pressure. The close proximity of the breathing ratio, and the Curie-Wiess temperature of $\text{CuAlCr}_4\text{S}_8$ to $\text{CuInCr}_4\text{S}_8$ may allow it to have similar complex nearest-neighbor magnetic interactions, switching from antiferromagnetic in smaller tetrahedra to ferromagnetic

in larger tetrahedra; however, *ab initio* calculations and neutron scattering experiments are required for a more accurate determination of the exchange interaction parameters and magnetic ground state, respectively. $\text{CuAlCr}_4\text{S}_8$ may present a clean realization of breathing pyrochlore physics due to the low antisite disorder and the fact that only one magnetic transition is observed.

ACKNOWLEDGMENTS

We would like to thank S. Dunsiger for her assistance during the μSR measurements. Work at McMaster was supported

by the Natural Sciences and Engineering Research Council of Canada. Portions of this work are based upon research conducted at the Center for High Energy X-ray Sciences (CHEXS), which is supported by the National Science Foundation under Award No. DMR-1829070. This research was undertaken owing, in part, to funding from the Max Planck-UBC-UTokyo Center for Quantum Materials and the Canada First Research Excellence Fund, Quantum Materials and Future Technologies Program. Work at University of Winnipeg was supported by Natural Sciences and Engineering Research Council of Canada (NSERC) and Canada Foundation for Innovation (CFI).

- [1] J. S. Gardner, M. J. P. Gingras, and J. E. Greedan, Magnetic pyrochlore oxides, *Rev. Mod. Phys.* **82**, 53 (2010).
- [2] H. R. Molavian, M. J. P. Gingras, and B. Canals, Dynamically Induced Frustration as a Route to a Quantum Spin Ice State in $\text{Tb}_2\text{Ti}_2\text{O}_7$ via Virtual Crystal Field Excitations and Quantum Many-Body Effects, *Phys. Rev. Lett.* **98**, 157204 (2007).
- [3] I. Mirebeau, A. Apetrei, J. Rodríguez-Carvajal, P. Bonville, A. Forget, D. Colson, V. Glazkov, J. P. Sanchez, O. Isnard, and E. Suard, Ordered Spin Ice State and Magnetic Fluctuations in $\text{Tb}_2\text{Sn}_2\text{O}_7$, *Phys. Rev. Lett.* **94**, 246402 (2005).
- [4] M. J. Harris, S. T. Bramwell, D. F. McMorrow, T. Zeiske, and K. W. Godfrey, Geometrical Frustration in the Ferromagnetic Pyrochlore $\text{Ho}_2\text{Ti}_2\text{O}_7$, *Phys. Rev. Lett.* **79**, 2554 (1997).
- [5] M. J. P. Gingras, C. V. Stager, N. P. Raju, B. D. Gaulin, and J. E. Greedan, Static Critical Behavior of the Spin-Freezing Transition in the Geometrically Frustrated Pyrochlore Antiferromagnet Spin Glass, *Phys. Rev. Lett.* **78**, 947 (1997).
- [6] L. Savary, K. A. Ross, B. D. Gaulin, J. P. C. Ruff, and L. Balents, Order by Quantum Disorder in $\text{Er}_2\text{Ti}_2\text{O}_7$, *Phys. Rev. Lett.* **109**, 167201 (2012).
- [7] S. H. Lee, H. Takagi, D. Louca, M. Matsuda, S. Ji, H. Ueda, Y. Ueda, T. Katsufuji, J. H. Chung, S. Park, S. W. Cheong, and C. Broholm, Frustrated magnetism and cooperative phase transitions in spinels, *J. Phys. Soc. Jpn.* **79**, 011004 (2010).
- [8] M. V. Talanov and V. M. Talanov, Formation of breathing pyrochlore lattices: Structural, thermodynamic and crystal chemical aspects, *CrystEngComm* **22**, 1176 (2020).
- [9] H. Duda, E. Maciążek, T. Groń, S. Mazur, A. W. Pacyna, A. Waśkowska, T. Mydlarz, and A. Gilewski, Spin-glass-like behavior in single-crystalline $\text{Cu}_{0.44}\text{In}_{0.48}\text{Cr}_{1.95}\text{Se}_4$, *Phys. Rev. B* **77**, 035207 (2008).
- [10] R. Plumier and M. Sougi, Magnetic ordering in the normal spinel $\text{Cu}_{0.5}\text{In}_{0.5}\text{Cr}_2\text{Se}_4$, *Solid State Commun.* **69**, 341 (1989).
- [11] R. Plumier, M. Sougi, and M. Lecomte, Observation of an unusual short range magnetic ordering in spinel $\text{Cu}_{1/2}\text{In}_{1/2}\text{Cr}_2\text{S}_4$, *Phys. Lett. A* **60**, 341 (1977).
- [12] D. Brasen, J. Vandenberg, M. Robbins, R. Willens, W. Reed, R. Sherwood, and X. Pinder, Magnetic and crystallographic properties of spinels of the type $\text{A}_x\text{B}_2\text{S}_4$ where $A = \text{Al, Ga}$, and $B = \text{Mo, V, Cr}$, *J. Solid State Chem.* **13**, 298 (1975).
- [13] C. Wilkinson, B. M. Knapp, and J. B. Forsyth, The magnetic structure of $\text{Cu}_{0.5}\text{Ga}_{0.5}\text{Cr}_2\text{S}_4$, *J. Phys. C* **9**, 4021 (1976).
- [14] H. M. Palmer and C. Greaves, Structural, magnetic and electronic properties of $\text{Fe}_{0.5}\text{Cu}_{0.5}\text{Cr}_2\text{S}_4$, *J. Mater. Chem.* **9**, 637 (1999).
- [15] H. D. Lutz, W. Becker, B. Müller, and M. Jung, Raman single crystal studies of spinel type MCr_2S_4 ($M = \text{Mn, Fe, Co, Zn, Cd}$), MIn_2S_4 ($M = \text{Mn, Fe, Co, Ni}$), $\text{MnCr}_{2-2x}\text{In}_{2x}\text{S}_4$ and $\text{Co}_{1-x}\text{Cd}_x\text{Cr}_2\text{S}_4$, *J. Raman Spectrosc.* **20**, 99 (1989).
- [16] G. J. Snyder, T. Caillat, and J. P. Fleurial, Thermoelectric properties of chalcogenides with the spinel structure, *Mater. Res. Innovations* **5**, 67 (2001).
- [17] G. J. Snyder, T. Caillat, and J. P. Fleurial, Thermoelectric properties of selenide spinels, *MRS Online Proc. Libr.* **626**, 33 (2000).
- [18] M. Gen, Y. Okamoto, M. Mori, K. Takenaka, and Y. Kohama, Magnetization process of the breathing pyrochlore magnet $\text{CuInCr}_4\text{S}_8$ in ultrahigh magnetic fields up to 150 T, *Phys. Rev. B* **101**, 054434 (2020).
- [19] A. N. Yaresko, Electronic band structure and exchange coupling constants in ACr_2X_4 spinels ($A = \text{Zn, Cd, Hg}$; $X = \text{O, S, Se}$), *Phys. Rev. B* **77**, 115106 (2008).
- [20] G. Pokharel, H. S. Arachchige, T. J. Williams, A. F. May, R. S. Fishman, G. Sala, S. Calder, G. Ehlers, D. S. Parker, T. Hong, A. Wildes, D. Mandrus, J. A. M. Paddison, and A. D. Christianson, Cluster Frustration in the Breathing Pyrochlore Magnet $\text{LiGaCr}_4\text{S}_8$, *Phys. Rev. Lett.* **125**, 167201 (2020).
- [21] P. Ghosh, Y. Iqbal, T. Müller, R. T. Ponnaganti, R. Thomale, R. Narayanan, J. Reuther, M. J. Gingras, and H. O. Jeschke, Breathing chromium spinels: a showcase for a variety of pyrochlore Heisenberg Hamiltonians, *npj Quantum Mater.* **4**, 63 (2019).
- [22] J. Hemberger, T. Rudolf, H.-A. Krug von Nidda, F. Mayr, A. Pimenov, V. Tsurkan, and A. Loidl, Spin-Driven Phonon Splitting in Bond-Frustrated ZnCr_2S_4 , *Phys. Rev. Lett.* **97**, 087204 (2006).
- [23] J. Hemberger, H.-A. Krug von Nidda, V. Tsurkan, and A. Loidl, Large Magnetostriction and Negative Thermal Expansion in the Frustrated Antiferromagnet ZnCr_2Se_4 , *Phys. Rev. Lett.* **98**, 147203 (2007).
- [24] G. Pokharel, A. F. May, D. S. Parker, S. Calder, G. Ehlers, A. Huq, S. A. J. Kimber, H. S. Arachchige, L. Poudel, M. A. McGuire, D. Mandrus, and A. D. Christianson, Negative thermal expansion and magnetoelastic coupling in the breathing pyrochlore lattice material $\text{LiGaCr}_4\text{S}_8$, *Phys. Rev. B* **97**, 134117 (2018).
- [25] R. Wawrzyńczak, Y. Tanaka, M. Yoshida, Y. Okamoto, P. Manuel, N. Casati, Z. Hiroi, M. Takigawa, and G. J. Nilsen, Classical Spin Nematic Transition in $\text{LiGa}_{0.95}\text{In}_{0.05}\text{Cr}_4\text{O}_8$, *Phys. Rev. Lett.* **119**, 087201 (2017).

- [26] R. Saha, R. Dhanya, C. Bellin, K. Béneut, A. Bhattacharyya, A. Shukla, C. Narayana, E. Suard, J. Rodríguez-Carvajal, and A. Sundaresan, Magnetostructural coupling and magnetodielectric effects in the A-site cation-ordered spinel $\text{LiFeCr}_4\text{O}_8$, *Phys. Rev. B* **96**, 214439 (2017).
- [27] D. Reig-i-Plessis and A. M. Hallas, Frustrated magnetism in fluoride and chalcogenide pyrochlore lattice materials, *Phys. Rev. Materials* **5**, 030301 (2021).
- [28] G. M. Kalvius, O. Hartmann, A. Krimmel, F. E. Wagner, R. Wäppling, V. Tsurkan, H.-A. K. von Nidda, and A. Loidl, Spin-lattice instability in the chromium sulfur spinel $\text{Fe}_{0.5}\text{Cu}_{0.5}\text{Cr}_2\text{S}_4$, *J. Phys.: Condens. Matter* **20**, 252204 (2008).
- [29] Y. Okamoto, G. J. Nilsen, T. Nakazono, and Z. Hiroi, Magnetic phase diagram of the breathing pyrochlore antiferromagnet $\text{LiGa}_{1-x}\text{In}_x\text{Cr}_4\text{O}_8$, *J. Phys. Soc. Jpn.* **84**, 043707 (2015).
- [30] Y. Okamoto, G. J. Nilsen, J. P. Attfield, and Z. Hiroi, Breathing Pyrochlore Lattice Realized in A-Site Ordered Spinel Oxides $\text{LiGaCr}_4\text{O}_8$ and $\text{LiInCr}_4\text{O}_8$, *Phys. Rev. Lett.* **110**, 097203 (2013).
- [31] Y. Tanaka, R. Wawrzyńczak, M. D. Le, T. Guidi, Y. Okamoto, T. Yajima, Z. Hiroi, M. Takigawa, and G. J. Nilsen, Inelastic neutron scattering study of the spin dynamics in the breathing pyrochlore system $\text{LiGa}_{0.95}\text{In}_{0.05}\text{Cr}_4\text{O}_8$, *J. Phys. Soc. Jpn.* **87**, 073710 (2018).
- [32] S. Lee, S.-H. Do, W. Lee, Y. S. Choi, J. Van Tol, A. P. Reyes, D. Gorbunov, W.-T. Chen, and K.-Y. Choi, Dichotomy in temporal and thermal spin correlations observed in the breathing pyrochlore $\text{LiGa}_{1-x}\text{In}_x\text{Cr}_4\text{O}_8$, *npj Quantum Mater.* **6**, 47 (2021).
- [33] H. Pinch, M. Woods, and E. Lopatin, Some new mixed A-site chromium chalcogenide spinels, *Mater. Res. Bull.* **5**, 425 (1970).
- [34] Y. Tazuke, Electric and magnetic properties of the system between Cr_3S_4 and VCr_2S_4 , *Phys. Lett. A* **69**, 341 (1979).
- [35] A. Suter and B. M. Wojek, Musrfit: A free platform-independent framework for μSR data analysis, *Phys. Proc.* **30**, 69 (2012).
- [36] Y. Okamoto, M. Mori, N. Katayama, A. Miyake, M. Tokunaga, A. Matsuo, K. Kindo, K. Takenaka *et al.*, Magnetic and structural properties of A-site ordered chromium spinel sulfides: Alternating antiferromagnetic and ferromagnetic interactions in the breathing pyrochlore lattice, *J. Phys. Soc. Jpn.* **87**, 034709 (2018).
- [37] T. Haku, M. Soda, M. Sera, K. Kimura, S. Itoh, T. Yokoo, and T. Masuda, Crystal field excitations in the breathing pyrochlore antiferromagnet $\text{Ba}_3\text{Yb}_2\text{Zn}_5\text{O}_{11}$, *J. Phys. Soc. Jpn.* **85**, 034721 (2016).
- [38] T. Kanematsu, M. Mori, Y. Okamoto, T. Yajima, and K. Takenaka, Thermal expansion and volume magnetostriction in breathing pyrochlore magnets LiACr_4X_8 ($A = \text{Ga, In}$, $X = \text{O, S}$), *J. Phys. Soc. Jpn.* **89**, 073708 (2020).
- [39] S. Lee, S.-H. Do, W.-J. Lee, Y. S. Choi, M. Lee, E. S. Choi, A. P. Reyes, P. L. Kuhns, A. Ozarowski, and K.-Y. Choi, Multistage symmetry breaking in the breathing pyrochlore lattice $\text{Li}(\text{Ga,In})\text{Cr}_4\text{O}_8$, *Phys. Rev. B* **93**, 174402 (2016).
- [40] I. M. Marshall, S. J. Blundell, F. L. Pratt, A. Husmann, C. A. Steer, A. I. Coldea, W. Hayes, and R. C. C. Ward, A muon-spin relaxation (μSR) study of the geometrically frustrated magnets $\text{Gd}_3\text{Ga}_5\text{O}_{12}$ and ZnCr_2O_4 , *J. Phys.: Condens. Matter* **14**, L157 (2002).